

Organic & Supramolecular Chemistry

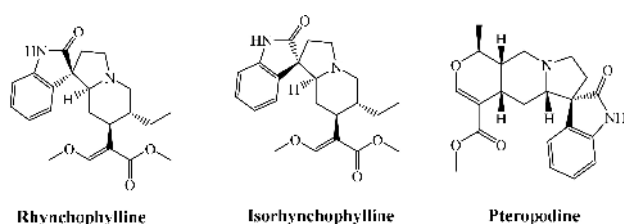
 γ -Fe₂O₃@SiO₂-EC-Zn^{II}: A Magnetic Recyclable Nanocatalyst for the Synthesis of Spiro[indoline-3, 9'-xanthene]trione Derivatives in Aqueous MediaMaryam Sadat Ghasemzadeh and Batool Akhlaghinia*^[a]

In this research, Zn^{II} immobilized on creatinated epibromohydrin functionalized γ -Fe₂O₃@SiO₂ nanoparticles (γ -Fe₂O₃@SiO₂-EC-Zn^{II}) as a novel magnetic nanostructured heterogeneous catalyst has been prepared readily and fully characterized by some spectroscopic and microscopic techniques such as fourier transform infrared spectroscopy (FT-IR), X-ray diffraction analysis (XRD), transmission electron microscopy (TEM), scanning electron microscopy (SEM), energy-dispersive X-ray spectroscopy (EDX), thermogravimetric analysis (TGA), vibrating sample magnetometry (VSM), dynamic light scattering (DLS), EDS-map, inductively coupled plasma atomic emission spectroscopy (ICP-OES) and CHNS. The above experimental results determined the composition of γ -Fe₂O₃@SiO₂-EC-Zn^{II} and clearly revealed

the core-shell structure nanoparticles are spherical in shape with the particle size in the range of 7–23 nm and superparamagnetic behavior. The magnetic nanostructured catalyst was identified as an efficient catalyst for the rapid synthesis of a library of spiro[indoline-3,9-xanthene]trione derivatives *via* the condensation reaction of different substituted isatins and dimedone or 1,3-cyclohexanedione at room temperature in aqueous media. Environmental friendliness, aqueous reaction medium, low cost, high yields, short reaction times, operational simplicity, wide applicability, magnetic recovery of catalyst and reusability up to seven cycles, as the important features of this protocol make the present methodology sustainable and economic.

Introduction

Recent developments in analysis of drugs show that polyfunctionalized heterocyclic compounds play an essential role in the drug discovery process.^[1,2] Therefore, interestingly a great deal of attention has been focused on the synthesis of heterocyclic compounds. The heterocyclic indole and indoline ring systems as key structural features are commonly found in a wide variety of pharmaceutical and biological active compounds (Scheme 1).^[3]

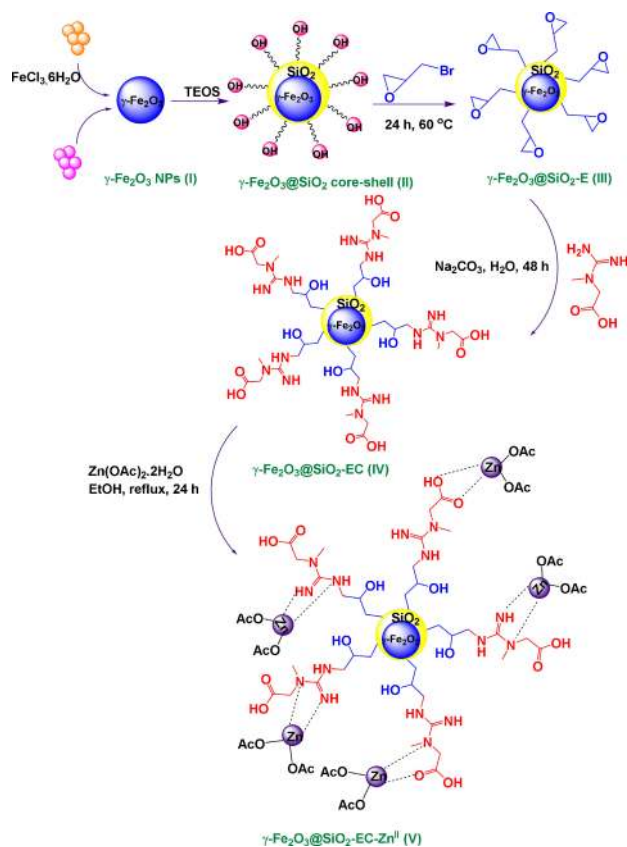


Scheme 1. The structure of bio-active compounds of indole.

Moreover, it has been reported that some indolines that are spiroannulated with heterocycles at the indole 3-carbon atom in isatin (sterically constrained spirooxindole ring system) have shown highly enhanced biological activity.^[4–7] Isatin and its derivatives due to their interesting biological properties are also used in organic synthesis extensively.^[5,8] Therefore, it is not surprising that a considerable interest in the synthesis of spirooxindole (especially spiro[indoline-3,9'-xanthene]trione) derivatives has been grown recently.^[9] Although, there are a few methods in the literature for the synthesis of spiro[indoline-3,9-xanthene]trione derivatives from isatin and dimedone.^[10–16] During last few years, the sustainable development of synthetic methodologies (with less environmental hazards) as a great challenge for chemical and medicinal researches has been provided selective access to the elaborated scaffolds combined with molecular diversity and eco-compatibility.^[17–19] In recent years, easy removal of catalyst from the reaction mixture, catalyst recovery and recyclability are the most important features for many catalytic processes. Hence, an efficient way to overcome the problem of homogeneous catalysts is creating a heterogeneous catalytic system through the heterogenization of active catalyst molecules.^[20] On the other hand, as the recovery of the most heterogeneous catalysts from the final reaction systems requires filtration or centrifugation step as a time consuming and tedious process, replacing magnetic separation by means of an external magnetic field can be a charming technique. Also, magnetic nanoparticles (MNPs) for use as supports enable environmentally friendly and sustainable catalytic processes. Because of the uncovered magnetic nanoparticles always tend to

[a] M. S. Ghasemzadeh, Prof. B. Akhlaghinia
Department of Chemistry, Faculty of Science, Ferdowsi University of
Mashhad, Mashhad 9177948974, Iran.
E-mail: akhlaghinia@um.ac.ir

Supporting information for this article is available on the WWW under
<https://doi.org/10.1002/slct.201703189>



Scheme 2. Preparation of Zn^{II} immobilized on creatinated epibromohydrin functionalized $\gamma\text{-Fe}_2\text{O}_3@SiO_2$ nanoparticles ($\gamma\text{-Fe}_2\text{O}_3@SiO_2\text{-EC-Zn}^{\text{II}}$ (V)).

aggregate into large clusters and thus lose their specific properties, the problem can be overcome by coating the nanoparticles with silica,^[21] polymer,^[22] carbon^[23] or metal oxide.^[24] Silica is commonly employed as the coating layer for the surface of MNPs, because it is inert, nontoxic, inexpensive, stable under catalytic conditions, has a high specific surface area as well as easy surface functionalization.^[25] Surface modification and grafting offer a broad range of approaches for constructing various magnetically recyclable nanostructured heterogeneous catalysts. Based on the above facts, Zn^{II} immobilized on creatinated epibromohydrin functionalized $\gamma\text{-Fe}_2\text{O}_3@SiO_2$ nanoparticles ($\gamma\text{-Fe}_2\text{O}_3@SiO_2\text{-EC-Zn}^{\text{II}}$) catalyst was prepared according to the procedure shown in Scheme 2. Coating of a layer of silica on the surface of $\gamma\text{-Fe}_2\text{O}_3$ (I) nanoparticles was achieved by stirring the $\gamma\text{-Fe}_2\text{O}_3$ suspension in deionized water with tetraethyl orthosilicate. Then, $\gamma\text{-Fe}_2\text{O}_3@SiO_2$ (II) was dispersed in pure epibromohydrine by sonication. Afterward the suspension was heated at 60 °C for 24 h to obtain $\gamma\text{-Fe}_2\text{O}_3@SiO_2\text{-E}$ (III). Subsequently, treatment of a suspension of $\gamma\text{-Fe}_2\text{O}_3@SiO_2\text{-E}$ (III) in deionized water with creatine monohydrate afforded $\gamma\text{-Fe}_2\text{O}_3@SiO_2\text{-EC}$ (IV). Creatine is a nitrogenous organic acid that occurs naturally in the human body and other vertebrates from glycine and arginine.^[26] Furthermore, it is a multidentate ligand so coordination of metal ions can be easily done into its sites. Finally $\gamma\text{-}$



Scheme 3. Synthesis of different structurally spiro[indoline-3,9'-xanthen]trione derivatives using $\gamma\text{-Fe}_2\text{O}_3@SiO_2\text{-EC-Zn}^{\text{II}}$ (V) in water.

$\text{Fe}_2\text{O}_3@SiO_2\text{-EC-Zn}^{\text{II}}$ (V) was obtained by the reaction of ethanolic solution of $\text{Zn}(\text{OAc})_2 \cdot 2\text{H}_2\text{O}$ with $\gamma\text{-Fe}_2\text{O}_3@SiO_2\text{-EC}$ (IV). In view of the important biological activity of spirooxindole derivatives and in continuation of our recent investigations into the synthesis of heterocyclic compounds under aqueous conditions,^[27–29] we targeted our study to find out eco-friendly and facile protocol for the synthesis of spiro[indoline-3,9'-xanthen]trione derivatives in the presence of $\gamma\text{-Fe}_2\text{O}_3@SiO_2\text{-EC-Zn}^{\text{II}}$ (V) (Scheme 3).

Results and Discussion

Characterization of catalyst

New $\gamma\text{-Fe}_2\text{O}_3@SiO_2\text{-EC-Zn}^{\text{II}}$ (V) as a magnetic nanocatalyst was prepared based on the method shown in Scheme 2. The composition of as-synthesized nanocatalyst was fully characterized using some different spectroscopic and microscopic techniques such as Fourier transform infrared (FT-IR) spectroscopy, X-ray diffraction analysis (XRD), transmission electron microscopy (TEM), scanning electron microscopy (SEM), energy-dispersive X-ray spectroscopy (EDX), thermogravimetric analysis (TGA), vibrating sample magnetometry (VSM), dynamic light scattering (DLS), EDS-map, inductively coupled plasma atomic emission spectroscopy (ICP-OES) and CHNS.

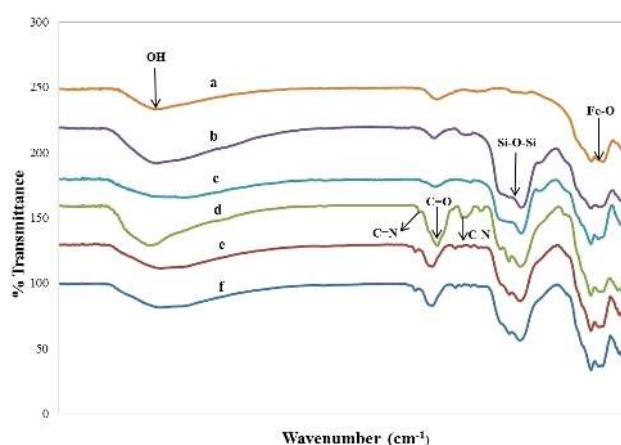


Figure 1. FT-IR spectra of (a) $\gamma\text{-Fe}_2\text{O}_3$ NPs (I), (b) $\gamma\text{-Fe}_2\text{O}_3@SiO_2$ core-shell (II), (c) $\gamma\text{-Fe}_2\text{O}_3@SiO_2\text{-E}$ (III), (d) $\gamma\text{-Fe}_2\text{O}_3@SiO_2\text{-EC}$ (IV), (e) $\gamma\text{-Fe}_2\text{O}_3@SiO_2\text{-EC-Zn}^{\text{II}}$ (V), (f) 7th recovered $\gamma\text{-Fe}_2\text{O}_3@SiO_2\text{-EC-Zn}^{\text{II}}$ (V).

Figure 1 indicates the FT-IR spectra of (a) γ -Fe₂O₃ NPs (I); (b) γ -Fe₂O₃@SiO₂ core-shell (II); (c) epibromohydrin functionalized γ -Fe₂O₃@SiO₂ (γ -Fe₂O₃@SiO₂-E) (III); (d) creatine monohydrate immobilized on epichlorohydrin functionalized γ -Fe₂O₃@SiO₂ (γ -Fe₂O₃@SiO₂-EC) (IV) and (e) Zn^{II} immobilized on creatinated epibromohydrin functionalized γ -Fe₂O₃@SiO₂ (γ -Fe₂O₃@SiO₂-EC-Zn^{II}) (V).

As can be seen, FT-IR spectrum of γ -Fe₂O₃ NPs (I) showed broad band at around 650–550 cm⁻¹, which was attributed to Fe–O vibration (Figure 1a).^[30] The stretching vibration of Si–O–Si bond in γ -Fe₂O₃@SiO₂ core-shell (II) can be observed as a strong broad band at 1099–1220 cm⁻¹.^[30] Furthermore, the absorption bands at 1625 cm⁻¹ and 3500–3100 cm⁻¹ were attributed to the bending and stretching vibrational modes of the physisorbed water and attached hydroxyl groups on the surface of γ -Fe₂O₃@SiO₂ core-shell (II) (Figure 1b). The grafted epoxy ring on γ -Fe₂O₃@SiO₂ core-shell (II) framework was recognized by the methylene C–H stretching and bending vibration bands at 2872–2920 and 1450 cm⁻¹, respectively. The intensity of the absorption band at 3500–3100 cm⁻¹ was decreased drastically due to the successful grafting of epoxy ring onto the γ -Fe₂O₃@SiO₂ core-shell (II). However an absorption band at 1110 cm⁻¹ was attributed to C–O–C vibrational stretching, which was covered by Si–O–Si band (Figure 1c). Ring opening of epoxy ring was performed by creatine monohydrate. Absorption bands at 1725 and 1639 cm⁻¹ related to C=N and C=O stretching vibrations respectively. As well, the band was depicted at 1450 cm⁻¹ in the spectrum of γ -Fe₂O₃@SiO₂-EC (IV) related to C–N stretching vibration frequency (Figure 1d). Also, Zn^{II} immobilized on creatinated epibromohydrin functionalized γ -Fe₂O₃@SiO₂ (γ -Fe₂O₃@SiO₂-EC-Zn^{II}) (V) was confirmed by decreasing the intensities of absorption bands of O–H, C=O and C–N bonds (Figure 1e).

XRD measurement was used to identify the crystalline structure of γ -Fe₂O₃@SiO₂-EC-Zn^{II} (V). As shown in (Figure 2), the XRD pattern exhibited reflection peaks at 2 Θ = 30°, 35.5°, 37°, 43°, 53.5°, 57°, 62.5°, 65.5°, 71°, 74° and 75° which can be indexed to (2 2 0), (3 3 1), (2 2 2), (4 0 0), (4 2 2), (5 1 1), (4 4 0), (5 3 1), (6 2 0), (5 3 3) and (6 2 2) reflections of the cubic structure of γ -Fe₂O₃ (JCPDS 13–664).^[31] In addition, the average

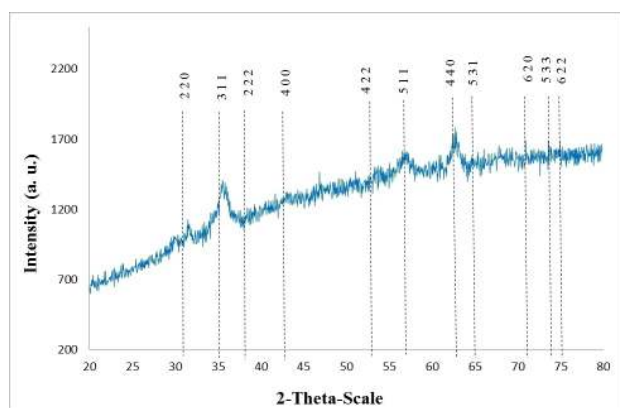


Figure 2. XRD pattern of γ -Fe₂O₃@SiO₂-EC-Zn^{II} (V).

crystallite size, *d*, of γ -Fe₂O₃@SiO₂-EC-Zn^{II} (V) calculated using the Debye–Scherrer equation $d = K \lambda / \beta \cos \theta$ is about 15 nm. Also, there is no obvious characteristic diffraction peaks associated to Zn(OH)₂ formation.^[32]

The morphology and size distribution of γ -Fe₂O₃@SiO₂-EC-Zn^{II} (V) was further determined using transmission electron microscopy (TEM), as shown in (Figure 3). TEM images showed that morphology of the most prepared nanoparticles are spherical in shape and also the size of particles is about 7–23 nm. Moreover, as can be seen the synthesized MNPs have core-shell structure. Furthermore, distribution histogram of γ -Fe₂O₃@SiO₂-EC-Zn^{II} (V) revealed that the average diameter of nanoparticles is 15 nm, which is in a good agreement with the results deduced from the XRD.

Surface morphology and size of the as-synthesized nanocatalyst, were investigated by scanning electron microscopy (SEM). SEM image of γ -Fe₂O₃@SiO₂-EC-Zn^{II} (V) reveals that the core-shell nanoparticles have spherical shape and the average particle sizes are 15 nm (Figure 4).

The energy dispersive spectrum (EDS) of γ -Fe₂O₃@SiO₂-EC-Zn^{II} (V) showed all of the expected elements C, O, N, Fe, Zn and Si (Figure 5). It is clear that creatine monohydrate was successfully immobilized on epibromohydrin functionalized γ -Fe₂O₃@SiO₂ (γ -Fe₂O₃@SiO₂-E) (III). Also no extra peaks related to any impurity are identified in the nanocatalyst structure.

Thermogravimetric analysis (TGA) was used to determine the thermal stability and the amount of organic moieties on the surface of γ -Fe₂O₃@SiO₂ core-shell (II). The TGA thermograms of γ -Fe₂O₃@SiO₂-E (III) (a), γ -Fe₂O₃@SiO₂-EC (IV) (b), γ -Fe₂O₃@SiO₂-EC-Zn^{II} (V) (c) are shown in Figure 6. The TGA of Fe₂O₃@SiO₂-E (III) (Figure 6a) shows two weight losses. The first step (81–173 °C, 1.91%) corresponds to the loss of adsorbed water on the surface of the nanoparticles. The second step (263–443 °C, 2.05%) is due to the loss of epibromohydrin on the surface of γ -Fe₂O₃@SiO₂ core-shell (II), thus the amount of organic segments is estimated to be 0.36 mmol g⁻¹. As can be noticed in Figure 6b, it is clear that the first decomposition step corresponds to the adsorbed water on the surface of γ -Fe₂O₃@SiO₂ core-shell (II) (93–174 °C, 1.69%). Removal of the organic segment happened at 400–459 °C (3.9%).

Accordingly, the amount of organic segments is estimated to be 0.24 mmol g⁻¹. The TGA thermogram of γ -Fe₂O₃@SiO₂-EC-Zn^{II} (V) is shown in Figure 6c. The first weight loss was also related to adsorbed water on the surface of nanocatalyst

Table 1. Thermogravimetric analysis (TGA) and elemental analysis (EA) results.

Samples	Percentage of weight loss (%)	Organic grafted segments (mmol g ⁻¹)	Elemental analysis (%) C N	
γ -Fe ₂ O ₃ @SiO ₂ -E (III)	2.05	0.36	1.11	-
γ -Fe ₂ O ₃ @SiO ₂ -EC (IV)	3.9	0.24	0.92	1.65
γ -Fe ₂ O ₃ @SiO ₂ -EC-Zn ^{II} (V)	4.21	0.189	1.02	1.68

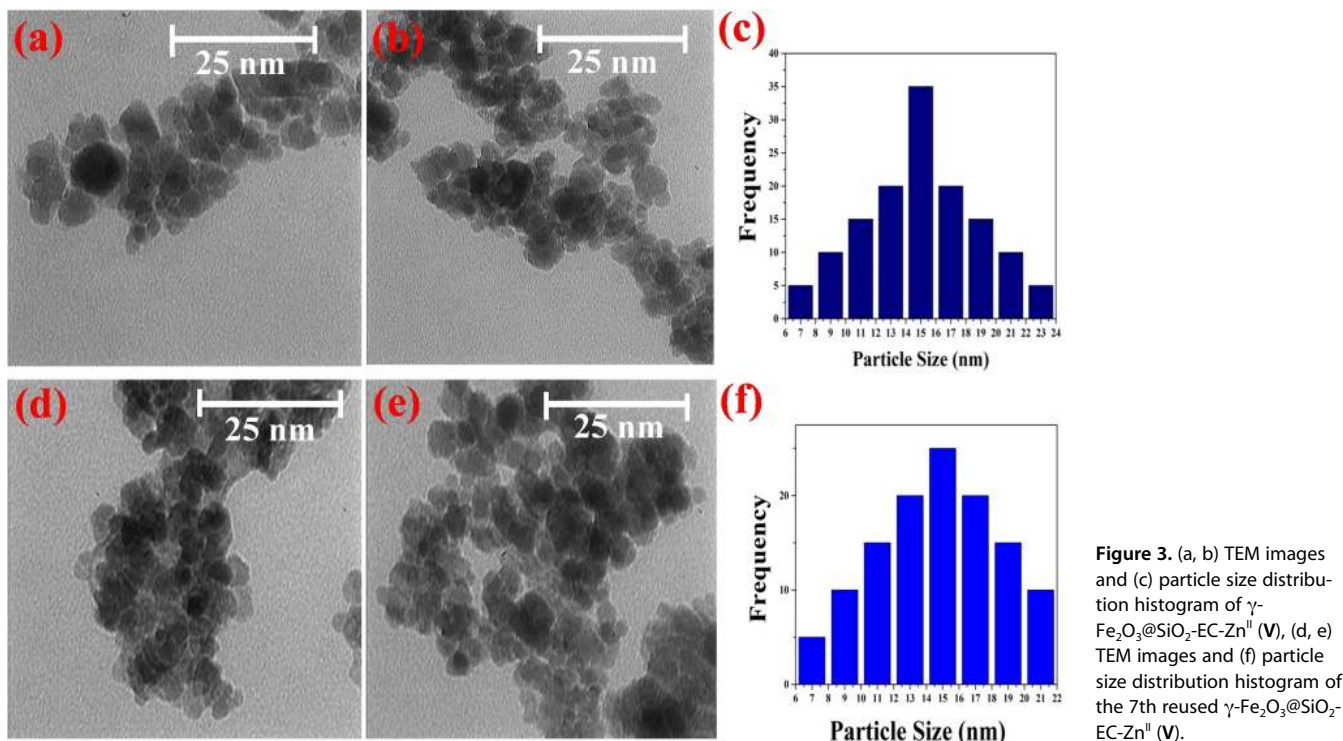


Figure 3. (a, b) TEM images and (c) particle size distribution histogram of $\gamma\text{-Fe}_2\text{O}_3\text{@SiO}_2\text{-EC-Zn}^{\text{II}}$ (V), (d, e) TEM images and (f) particle size distribution histogram of the 7th reused $\gamma\text{-Fe}_2\text{O}_3\text{@SiO}_2\text{-EC-Zn}^{\text{II}}$ (V).

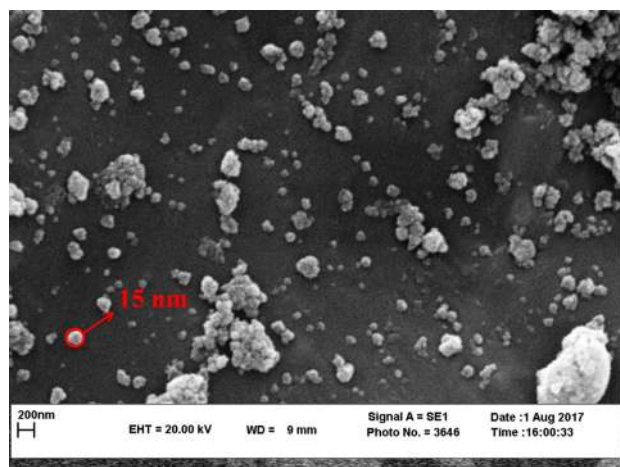


Figure 4. The SEM image of $\gamma\text{-Fe}_2\text{O}_3\text{@SiO}_2\text{-EC-Zn}^{\text{II}}$ (V).

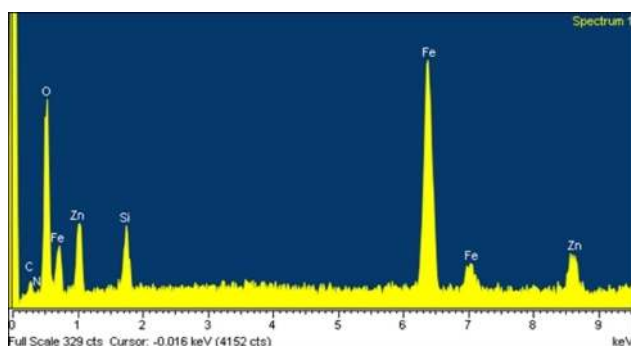


Figure 5. The EDS analysis of $\gamma\text{-Fe}_2\text{O}_3\text{@SiO}_2\text{-EC-Zn}^{\text{II}}$ (V).

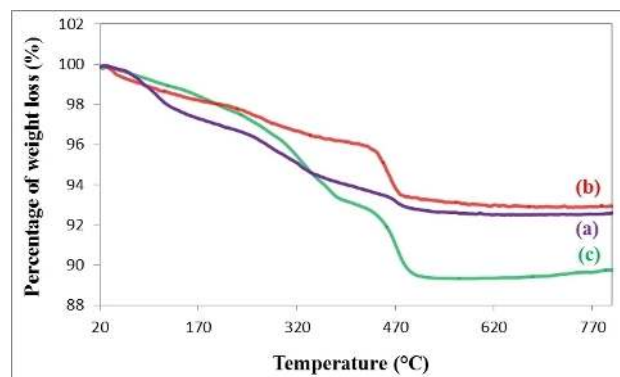


Figure 6. TGA thermograms of (a) $\gamma\text{-Fe}_2\text{O}_3\text{@SiO}_2\text{-E}$ (III), (b) $\gamma\text{-Fe}_2\text{O}_3\text{@SiO}_2\text{-EC}$ (IV) and (c) $\gamma\text{-Fe}_2\text{O}_3\text{@SiO}_2\text{-EC-Zn}^{\text{II}}$ (V).

happened at 129–210 °C (0.74%). The main weight loss (4.21%) at 373–520 °C could be assigned to the organic segments grafted on the surface of the nanocatalyst. According to the TGA data, the amount of organic segments supported on $\gamma\text{-Fe}_2\text{O}_3\text{@SiO}_2$ (II) is estimated to be 0.189 mmol g^{-1} . Good agreement was observed between the elemental analysis and TGA data, according to the results summarized in Table 1.

Besides, the total zinc content in the freshly prepared catalyst which was determined by ICP-OES analysis is calculated to be 230122 ppm, 0.23 g or 0.0004 mmol of Zn^{II} per 1.00 g of nanocatalyst. The magnetization curve of $\gamma\text{-Fe}_2\text{O}_3\text{@SiO}_2\text{-EC-Zn}^{\text{II}}$ (V) was measured at ambient temperature by a vibrating sample magnetometry (VSM). As illustrated in (Figure 7), the value of saturation magnetic moments of $\gamma\text{-Fe}_2\text{O}_3\text{@SiO}_2\text{-EC-Zn}^{\text{II}}$ (V) is $M_s = 30.65 \text{ emu g}^{-1}$ which was lower than the value for $\gamma\text{-Fe}_2\text{O}_3$.

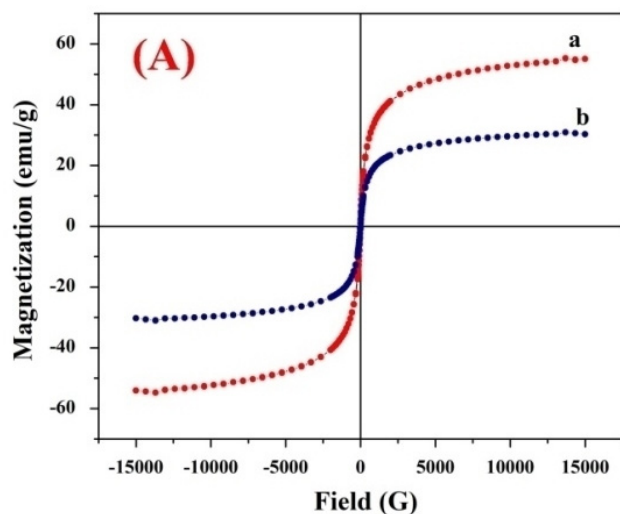


Figure 7. (A) Magnetization curves of (a) $\gamma\text{-Fe}_2\text{O}_3$ and (b) $\gamma\text{-Fe}_2\text{O}_3\text{@SiO}_2\text{-EC-Zn}^{\text{II}}$ (V), (B) Catalyst ability for effective recovery at the end of reactions by an external magnetic field.

Fe_2O_3 particles $M_s = 55.58 \text{ emu g}^{-1}$. Decreasing in the saturation magnetization of $\gamma\text{-Fe}_2\text{O}_3\text{@SiO}_2\text{-EC-Zn}^{\text{II}}$ (V) after surface grafting, can be attributed to the contribution of the non-magnetic materials.

The dynamic light scattering (DLS) technique was carried out to determine the particle size distribution of the $\gamma\text{-Fe}_2\text{O}_3\text{@SiO}_2\text{-EC-Zn}^{\text{II}}$ (V) (Figure 1). As can be concluded from Figure 8, the value of the obtained sample indicates that the median size of 99% $\gamma\text{-Fe}_2\text{O}_3\text{@SiO}_2\text{-EC-Zn}^{\text{II}}$ (V) are about 7–23 nm which is in good agreement with the data obtained from the TEM and SEM analysis. The corresponding EDS-map images of (a) $\gamma\text{-Fe}_2\text{O}_3\text{@SiO}_2\text{-E}$ (III), (b) $\gamma\text{-Fe}_2\text{O}_3\text{@SiO}_2\text{-EC}$ (IV) and (c) $\gamma\text{-Fe}_2\text{O}_3\text{@SiO}_2\text{-EC-Zn}^{\text{II}}$ (V) indicated that C, N, S, O, Fe, Si and Zn were dispersed uniformly on the surface of magnetite nanoparticles (Figure 9a, b and c).

Synthesis of spiro[indoline-3,9'-xanthen]trione derivatives in the presence of $\gamma\text{-Fe}_2\text{O}_3\text{@SiO}_2\text{-EC-Zn}^{\text{II}}$ (V). To show the merit of $\gamma\text{-Fe}_2\text{O}_3\text{@SiO}_2\text{-EC-Zn}^{\text{II}}$ (V) and in view of the important pharmaceutical and biological activities of indole derivatives, we embarked our attention towards finding an efficient, facile and environmental benign synthetic methodology for the

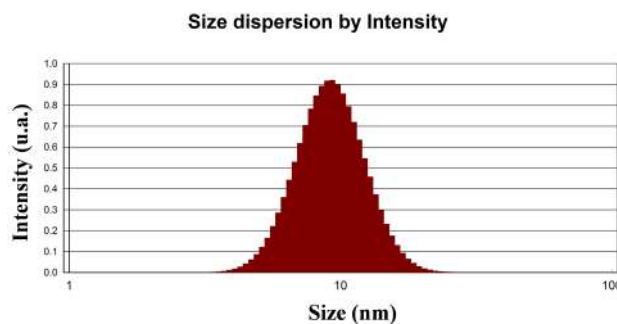


Figure 8. DLS analysis of $\gamma\text{-Fe}_2\text{O}_3\text{@SiO}_2\text{-EC-Zn}^{\text{II}}$ (V).

synthesis of spiro[indoline-3,9'-xanthen]trione derivatives. At the onset, using the synthesis of 3',3',6',6'-tetramethyl-3',4',6',7'-tetrahydrospiro[indoline-3,9'-xanthen]-1',2,8'(2'H,5'H)-trione as a model reaction, the reaction conditions were optimized with respect to the presence or absence of the catalyst, temperature, solvents and catalyst loading. The results are summarized in Table 2.

In continuation of our recent studies aimed at developing eco-friendly protocols in organic synthesis^[24, 33–52] and based on R. A. Sheldon statement “the best solvent is no solvent and if a solvent (diluent) is needed it should preferably be water”^[53] we carried out the model reaction in solvent free condition / and or employing water as the reaction medium at 80 °C by taking 1/2 molar ratio of isatin/dimedone respectively.

As it was shown in Table 2, without catalyst, no expected product was obtained even after prolonged stirring (Table 2, entries 1–2). At the same reaction conditions, a trace amount of desired product was obtained in refluxing H_2O (Table 2, entry 3). Interestingly, applying 1 mol% of $\gamma\text{-Fe}_2\text{O}_3\text{@SiO}_2\text{-EC-Zn}^{\text{II}}$ (V) afforded 3',3',6',6'-tetramethyl-3',4',6',7'-tetrahydrospiro[indoline-3,9'-xanthen]-1',2,8'(2'H,5'H)-trione in high yield (Table 2, entry 4).

Subsequent experiment led to the finding that a reasonable yield of desired product can be gained at room temperature (Table 2, entry 5). In the course of our research and evaluation of different catalyst loading, we have found that rate enhancement of the reaction was observed by applying 2.5 mol% of catalyst and excellent yield of desired product was afforded (Table 2, entries 6–11).

Next, to further determine the true catalyst species for the preparation of 3',3',6',6'-tetramethyl-3',4',6',7'-tetrahydrospiro[indoline-3,9'-xanthen]-1',2,8'(2'H,5'H)-trione, the model reaction was performed under the identical conditions in the presence of $\gamma\text{-Fe}_2\text{O}_3$ NPS (I), $\gamma\text{-Fe}_2\text{O}_3\text{@SiO}_2$ core-shell (II), $\gamma\text{-Fe}_2\text{O}_3\text{@SiO}_2\text{-E}$ (III), $\gamma\text{-Fe}_2\text{O}_3\text{@SiO}_2\text{-EC}$ (IV) and $\text{Zn}(\text{OAc})_2\cdot 2\text{H}_2\text{O}$ respectively (Table 2, entries 12–16).

Table 2 indicates that the reaction did not occur efficiently and even after long period of time low yield of product was gained. For comparison, the model reaction has also been carried out in different solvents like EtOH, PEG, DMF, DMSO, CH_3CN , 1,4-dioxane and THF (Table 2, entries 17–23). It was

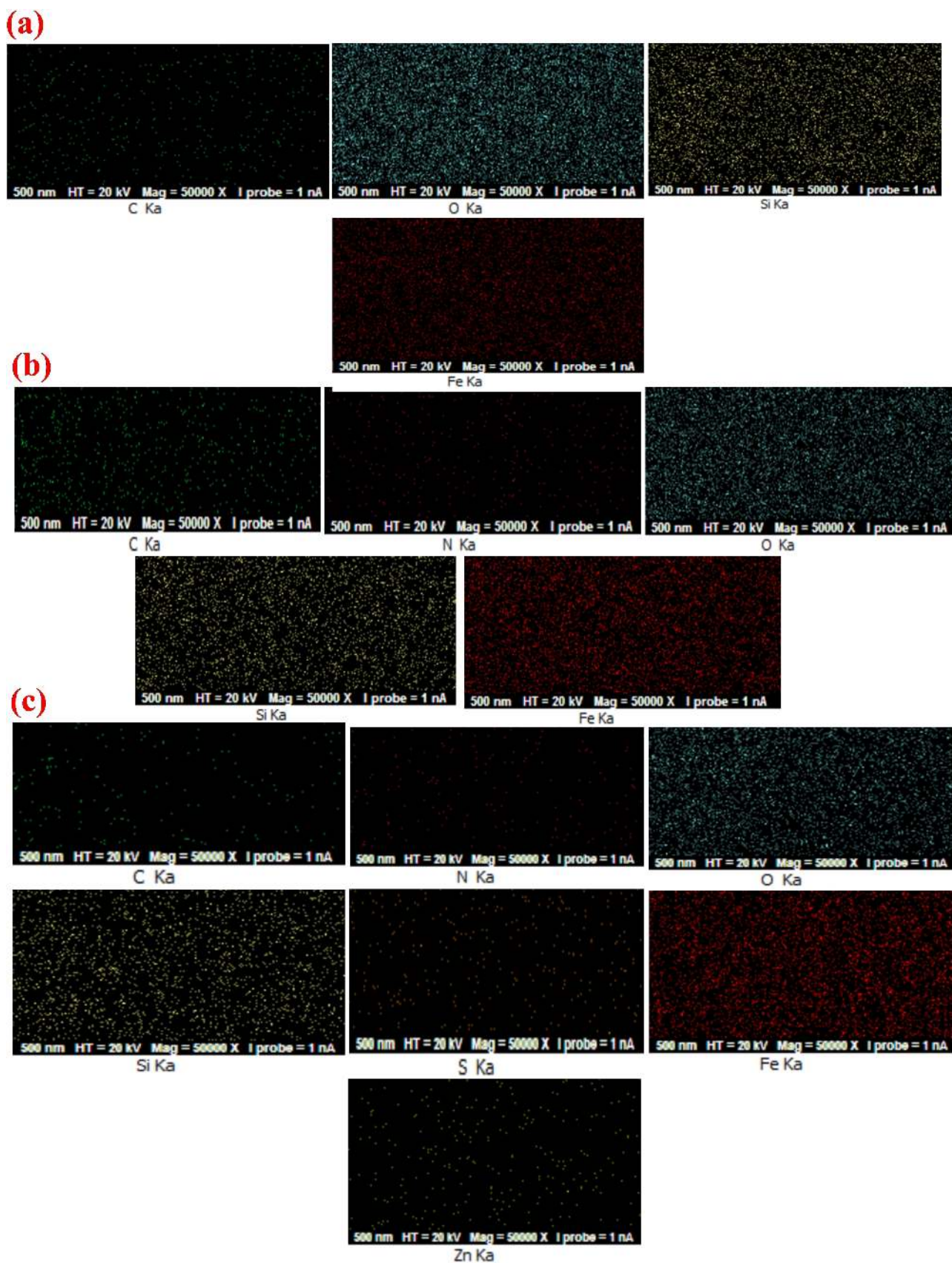


Figure 9. EDS-map images of (a) $\gamma\text{-Fe}_2\text{O}_3/\text{SiO}_2\text{-E}$ (III), (b) $\gamma\text{-Fe}_2\text{O}_3/\text{SiO}_2\text{-EC}$ (IV) and (c) $\gamma\text{-Fe}_2\text{O}_3/\text{SiO}_2\text{-EC-Zn}^{\text{II}}$ (V).

Table 2. Optimization of various reaction parameters for the synthesis of 3',3',6',6'-tetramethyl-3',4',6',7'-tetrahydrospiro[indoline-3,9'-xanthen]-1',2,8'(2'H,5'H)-trione in the presence of $\gamma\text{-Fe}_2\text{O}_3\text{@SiO}_2\text{-EC-Zn}^{\text{II}}$ (V).

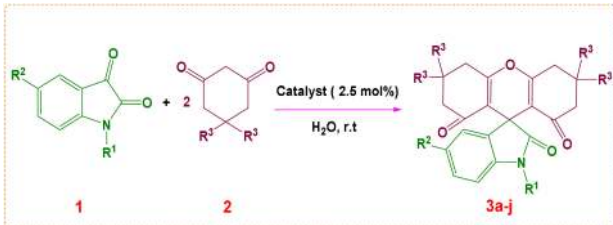
Entry	Amount of catalyst (mol%)	Solvent	Temperature (°C)	Time (min)	Isolated Yield (%)
1	-	-	80	24(h)	0
2	-	H ₂ O	80	24 (h)	0
3	-	H ₂ O	reflux	24 (h)	trace
4	1	H ₂ O	reflux	35	95
5	1	H ₂ O	r.t.	55	95
6	1.2	H ₂ O	r.t.	50	95
7	1.4	H ₂ O	r.t.	40	95
8	1.5	H ₂ O	r.t.	30	95
9	2	H ₂ O	r.t.	15	95
10	2.5	H ₂ O	r.t.	5	95
11	3	H ₂ O	r.t.	5	95
12 ^a	2.5	H ₂ O	r.t.	2/24 (h)	10/40
13 ^b	0.06 (g)	H ₂ O	r.t.	2/24 (h)	15/45
14 ^c	0.06 (g)	H ₂ O	r.t.	2/24 (h)	15/48
15 ^d	0.06 (g)	H ₂ O	r.t.	2/24 (h)	25/55
16 ^e	2.5	H ₂ O	r.t.	2/24 (h)	30/40
16	2.5	EtOH	r.t.	1/24 (h)	50/80
17	2.5	PEG	r.t.	3/24 (h)	20/70
18	2.5	DMF	r.t.	2/24 (h)	50/75
19	2.5	DMSO	r.t.	3/24 (h)	20/35
20	2.5	CH ₃ CN	r.t.	2/24 (h)	30/55
21	2.5	1,4-Dioxane	r.t.	2/24 (h)	10/40
22	2.5	THF	r.t.	3/24 (h)	5/30

^a The reaction was performed in the presence of $\gamma\text{-Fe}_2\text{O}_3$ NPs (I). ^b The reaction was performed in the presence of $\gamma\text{-Fe}_2\text{O}_3\text{@SiO}_2$ core-shell (II). ^c The reaction was performed in the presence of $\gamma\text{-Fe}_2\text{O}_3\text{@SiO}_2\text{-E}$ (III). ^d The reaction was performed in the presence of $\gamma\text{-Fe}_2\text{O}_3\text{@SiO}_2\text{-EC}$ (IV). ^e The reaction was performed in the presence of $\text{Zn}(\text{OAc})_2\cdot 2\text{H}_2\text{O}$.

found that H₂O has shown superiority over the other solvents which sufficiently push the reaction forward.

After optimization of the reaction conditions, the general efficiency of this protocol was then delineated for the synthesis of a variety of spiro[indoline-3,9'-xanthen]trione derivatives in regard to library construction by using different substituted isatins and dimedone or 1,3-cyclohexanedione. The results are summarized in Table 3. All the reactions were completed rapidly with acceptable yields. In comparison, the results of Table 3 demonstrated that dimedone reacted more quickly than 1,3-cyclohexanedione and afforded the desired products in shorter reaction times (Table 3, entries 1–6 vs entries 7–10). Thus, it is reasonable to conclude that dimedone as a methylene compound is more reactive than 1,3-cyclohexane-

Table 3. Synthesis of different structurally spiro[indoline-3,9'-xanthen]trione derivatives in the presence of $\gamma\text{-Fe}_2\text{O}_3\text{@SiO}_2\text{-EC-Zn}^{\text{II}}$ (V).



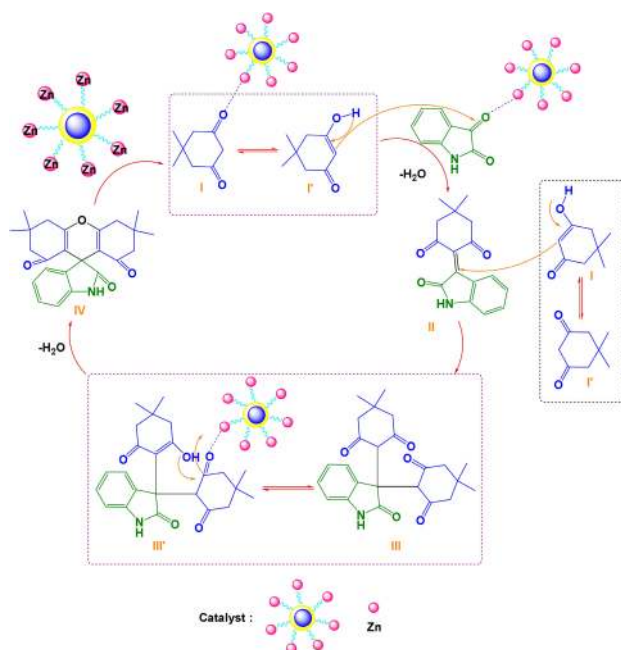
Entry	R ¹	R ²	R ³	Product	Time (min)	Yield (%)
1	H	H	Me	3a	5	95
2	Me	Me	Me	3b	15	90
3	H	Me	Me	3c	10	94
4	H	OMe	Me	3d	8	93
5	H	Cl	Me	3e	12	95
6	H	NO ₂	Me	3f	18	90
7	H	H	H	3 g	10	95
8	H	Me	H	3 h	15	95
9	H	OMe	H	3i	12	92
10	H	Cl	H	3j	18	95

dione in preparation of spiro[indoline-3,9'-xanthen]trione derivatives in the presence of $\gamma\text{-Fe}_2\text{O}_3\text{@SiO}_2\text{-EC-Zn}^{\text{II}}$ (V).

Some of synthesized spiro[indoline-3,9'-xanthen]trione derivatives (3a, 3e, 3f, 3g, 3j) are known and their structures were established by comparison of their melting points and mass spectrometry with those of authentic samples. Molecular ion peaks of all products were apparent at their respective *m/z* in mass spectrometry. The FT-IR, ¹H NMR and ¹³C NMR spectra of some selected compounds were in a good agreement with the data reported in the literature. The structure of the novel compounds (3b, 3c, 3d, 3h, 3i) were also established by elemental analysis data. Completion of the reaction was confirmed by disappearance of reactants and formation of desired product on TLC. Appearance of two absorption bands at 1168 and 1617 cm⁻¹ related to stretching vibrations of C–O–C and C=C definitely recognized the formation of spiro[indoline-3,9'-xanthen]trione derivatives.

Also, strong absorption bands at 1739–1733, 1715–1623 and 1666–1622 cm⁻¹ due to carbonyl groups obviously disclosed the conjugation with olefinic bonds and NH respectively in spiro[indoline-3,9'-xanthen]triones structures. The ¹H NMR spectra exhibited two singlet signals of 4CH₃ at δ 1.14–1.11 and 1.07–1.04 ppm. Signals of eight protons (4CH₂) appeared at 2.61–2.12 ppm as two doublets. Moreover, the proposed product structure was revealed by the requisite number of 16–18 distinct resonances in the ¹³C NMR spectra. Resonating signals at 178–177, 195–195.50 and 172.85–163.45 ppm related to spiro carbon, conjugated carbonyl with C=C bond and carbonyl group of isatin ring system respectively.

The probable $\gamma\text{-Fe}_2\text{O}_3\text{@SiO}_2\text{-EC-Zn}^{\text{II}}$ (V) catalyzed mechanistic pathway for the synthesis of spiro[indoline-3,9'-xanthen]trione derivatives is depicted in Scheme 4 on the basis of the similar reactions of isatin.^[13] According the results of Table 2 (entries 1–3) the Lewis acidity of the catalyst has an essential



Scheme 4. Proposed reaction mechanism for the synthesis of spiro[indoline-3,9'-xanthen]trione derivatives in the presence of $\gamma\text{-Fe}_2\text{O}_3\text{@SiO}_2\text{-EC-Zn}^{\text{II}}$ (V).

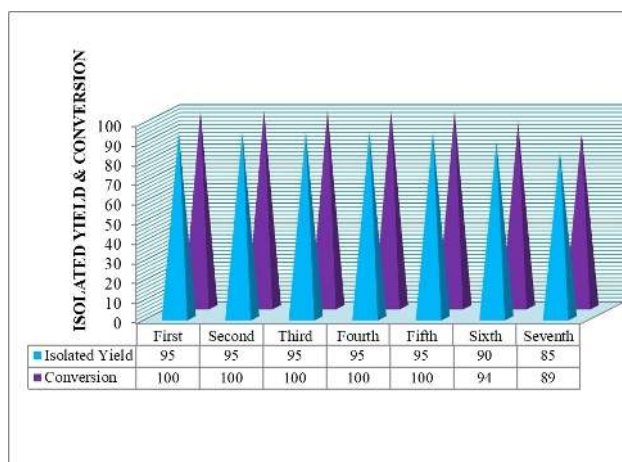


Figure 10. Synthesis of 3',3',6',6'-tetramethyl-3',4',6',7'-tetrahydrospiro[indoline-3,9'-xanthen]-1',2,8'(2'H,5'H)-trione in the presence of reused $\gamma\text{-Fe}_2\text{O}_3\text{@SiO}_2\text{-EC-Zn}^{\text{II}}$ (V).

role in the promotion of the condensation reaction. It is believed that, Lewis acidic sites (Zn^{II}) of nanocatalyst activated isatin towards the nucleophilic attack of activated dimesone or 1,3-cyclohexanedione upon enolization (two tautomeric forms I and I'). (The interaction of nanocatalyst with isatin and dimesone were confirmed with shifting of $\text{C}=\text{O}$ groups to lower frequencies in FT-IR spectrum. (see supporting information)). After dehydration, the aldol adduct II was afforded. (Further investigation on the elucidation of the mechanism was undertaken by performing the simultaneous reaction of isatin with dimesone under optimized reaction conditions at -10°C .

The intermediate II was separated and the physical and chemical properties were confirmed according to the literature, (m.p. $> 250^\circ\text{C}$).^[54] (see supporting information)).

In the next step, Michael addition led to formation of III which was in tautomeric equilibration with III' in the presence of nanocatalyst. Subsequently, intramolecular cyclization which was followed by dehydration produced the desired product. In the following, $\gamma\text{-Fe}_2\text{O}_3\text{@SiO}_2\text{-EC-Zn}^{\text{II}}$ (V) was released from the product and re-entered the catalytic cycle. More investigations to clarify the mechanism in details are currently underway in our laboratory.

The recyclability of our magnetic catalyst was explored using the model reaction of isatin and dimesone under the optimized reaction conditions. After each run, the catalyst was separated simply *via* attaching an external magnet onto the reaction vessel and washed with boiling EtOAc. Then, the nanocatalyst was reused for next run after drying at ambient temperature. In a set of 7 successive recycle runs, the catalytic activity of $\gamma\text{-Fe}_2\text{O}_3\text{@SiO}_2\text{-EC-Zn}^{\text{II}}$ (V) was restored without appreciable loss of its catalytic activity. Within the limits of the experimental errors, up to 97% of catalyst could be recovered from each run (Figure 10). Although during the recovery process of the catalyst, no significant deterioration of absorption bands in FT-IR spectrum of the catalyst was displayed (Figure 1f).

ICP-OES analysis showed that freshly prepared catalyst contains 230122 ppm, 0.23 g or 0.0004 mmol of Zn^{II} per 1.00 g of the catalyst, while the 7th reused catalyst contains 198974 ppm, 0.19 g or 0.0003 mmol of Zn^{II} per 1.00 g of the catalyst.

It indicates that 83% of Zn^{II} could be found in the structure of the catalyst after seven runs. In addition, to check the heterogeneous nature and leaching out of zinc metal from $\gamma\text{-Fe}_2\text{O}_3\text{@SiO}_2\text{-EC-Zn}^{\text{II}}$ (V) catalyst, hot filtration test was carried out.^[55] For this purpose the hot-filtration test was conducted on model reaction according to a typical procedure (Figure 11).

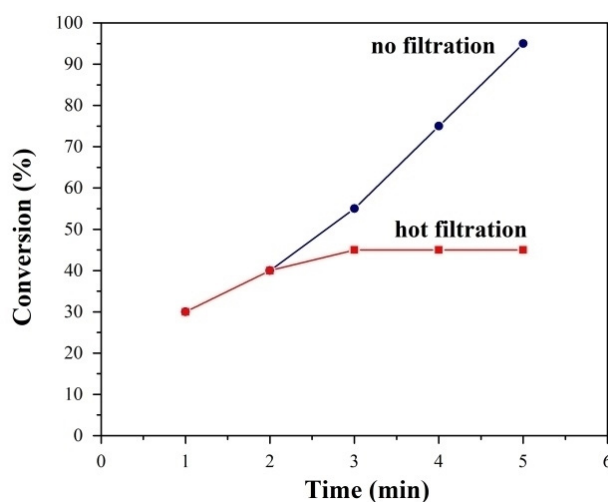


Figure 11. Hot filtration experiment for model reaction using $\gamma\text{-Fe}_2\text{O}_3\text{@SiO}_2\text{-EC-Zn}^{\text{II}}$ (V).

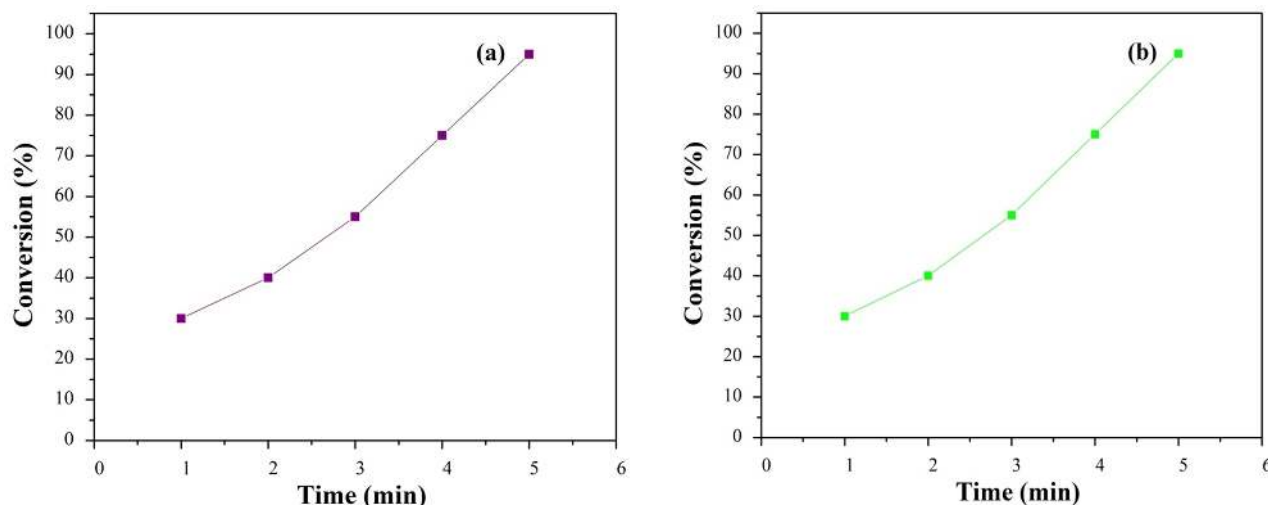


Figure 12. Product conversion as a function of reaction time catalyzed by $\gamma\text{-Fe}_2\text{O}_3\text{@SiO}_2\text{-EC-Zn}^{\text{II}}$ (V) in (a) the absence and (b) the presence of EDTA.

Table 4. Comparison between efficiency of $\gamma\text{-Fe}_2\text{O}_3\text{@SiO}_2\text{-EC-Zn}^{\text{II}}$ (V) and some other catalysts for the synthesis of 3',3',6',6'-tetramethyl-3',4',6',7'-tetrahydrospiro[indoline-3,9'-xanthene]-1',2,8'(2'H,5'H)-trione.

Entry	Catalyst	Solvent	Temperature (°C)	Time (min)	Yield (%)	Ref.
1	SBA-15-Pr-SO ₃ H	-	130	20	90	11
2	Neutral Alumina	MeOH	r.t	30	88	13
3 ^a	<i>p</i> -TSA	H ₂ O	reflux	24 (h)	75	10
4	-	EtOH then AcOH	reflux	12 (h)	92	56
5	-	AcOH	reflux	4 (h)	70	57
6	ZnO	-	100	2 (h)	85	12
7 ^b	-	LTTM	90	30	85	15
8	$\gamma\text{-Fe}_2\text{O}_3\text{@SiO}_2\text{-EC-Zn}^{\text{II}}$ (V)	H ₂ O	r.t	5	95	Present study

^a *p*-Toluenesulfonic acid. ^b Oxalic acid dihydrate: proline.

First, the reaction was allowed to proceed for about 2.5 minutes. The nanocatalyst was then separated from the reaction mixture with a magnet while the mother liquor stayed and reacted for an extended duration (for another 15 min) under identical conditions. The conversion was monitored by thin layer chromatography at different times. Figure 11 illustrated no further progress in condensation reaction. However, it is known that the negative hot filtration test alone cannot prove that the reaction occurs heterogeneously, because the leached metal can re-deposit so quickly that it may not be detected by a filtration test.^[55]

Also, the heterogeneity of a catalyst is often checked by catalyst poisoning experiment. So this experiment was performed in synthesis of spiro[indoline-3,9'-xanthene]trione derivatives in aqueous media in the presence of $\gamma\text{-Fe}_2\text{O}_3\text{@SiO}_2\text{-EC-Zn}^{\text{II}}$ (V) and EDTA (250 mg) with gentle magnetic stirring at room temperature. The reaction was monitored by thin layer chromatography analysis for five times. The results did not show suppression of the catalytic activity, so complete conversion was observed (Figure 12).

To gain insight into the proficiency of $\gamma\text{-Fe}_2\text{O}_3\text{@SiO}_2\text{-EC-Zn}^{\text{II}}$ (V) in the synthesis of spiro[indoline-3,9'-xanthene]trione derivatives, we compared its catalytic activity with some of the

earlier reported catalysts in literature (Table 4). It is clear that $\gamma\text{-Fe}_2\text{O}_3\text{@SiO}_2\text{-EC-Zn}^{\text{II}}$ (V) forwarded the reaction more quickly than the methods described previously.

Furthermore, in the presence of our magnetic nanocatalyst, high yield of desired product was obtained in H₂O as green media (compare with entries 2, 4, 5) and at room temperature as well (compare with entries 1, 2–7). Besides the above mentioned advantages, magnetically separation of catalyst from the reaction mixture provides easy and less time-consuming work-up procedure as the key feature of this study when compared with other existing methods.

Conclusions

In summary, Zn^{II} immobilized on creatinated epibromohydrin functionalized $\gamma\text{-Fe}_2\text{O}_3\text{@SiO}_2$ nanoparticles ($\gamma\text{-Fe}_2\text{O}_3\text{@SiO}_2\text{-EC-Zn}^{\text{II}}$ (V)) facilitated the rapid synthesis of spiro[indoline-3,9'-xanthene]trione derivatives in green media. Characterization results validate that magnetic nanocatalyst $\gamma\text{-Fe}_2\text{O}_3\text{@SiO}_2\text{-EC-Zn}^{\text{II}}$ (V) with spherical shape and mean diameters of 7–23 nm was successfully synthesized. Also these results validate that no agglomeration or increase in the particle size was observed even after 7 consecutive recycle runs.

The present eco-compatible synthetic methodology was devoid of tedious work-up and afforded the analytically pure desired products in excellent yields through a single recrystallization step in EtOH/H₂O. Moreover, catalyst recycling was easily accomplished with the assistance of the external magnet. The catalyst can be recycled up to seven times without a substantial reduction in its catalytic activity. We believe that the utility of this synthetic methodology (as a more practical alternative to the other existing method) is highly promising, provides a better scope for the preparation of spiro[indoline-3,9'-xanthen]trione derivatives with ecological benefits and will be a good contribution in innovation of green chemistry.

Supporting Information Summary

Experimental section, FT-IR, ¹H NMR, ¹³C NMR, Mass spectrum and CHNS analysis of products were described.

Acknowledgements

The authors gratefully acknowledge the partial support of this study by Ferdowsi University of Mashhad Research Council (Grant no. p/3/43366).

Conflict of Interest

The authors declare no conflict of interest.

Keywords: aqueous media · creatine monohydrate · heterogeneous nanocatalyst · spiro[indoline-3,9'-xanthen]trione derivatives

- [1] A. Dömling, I. Ugi, *Angew. Chem. Int. Ed.* **2000**, *112*, 3300–3344.
- [2] A. Dömling, *Chem. Rev.* **2006**, *106*, 17–89.
- [3] R. J. Sundberg, *The Chemistry of Indoles*, Academic New York, **1996**.
- [4] K. C. Joshi, P. Chand, *Pharmazie* **1982**, *37*, 1–12.
- [5] J. F. M. Da Silva, S. J. Garden, A. C. Pinto, *J. Braz. Chem. Soc.* **2001**, *12*, 273–324.
- [6] A. H. Abdel-Rahman, E. M. Keshk, M. A. Hanna, S. M. El-Bady, *Bioorg. Med. Chem.* **2004**, *12*, 2483–2488.
- [7] S. L. Zhu, S. J. Ji, Z. Yong, *Tetrahedron* **2007**, *63*, 9365–9372.
- [8] N. Lashgari, G. Mohammadi Ziarani, *Arkivoc* **2012**, *1*, 277–320.
- [9] A. J. Kell, D. L. B. Stringle, M. S. Workentin, *Org. Lett.* **2000**, *2*, 3381–3384.
- [10] S. Ahadi, H. R. Khavasi, A. Bazgir, *Chem. Pharm. Bull.* **2008**, *56*, 1328–1330.
- [11] G. Mohammadi Ziarani, N. Lashgari, A. R. Badiei, *Sci. Iran.* **2013**, *20*, 580–586.
- [12] J. Kothandapani, A. Ganesan, G. K. Mani, A. J. Kulandaisamy, J. B. B. Rayappan, S. S. Ganesan, *Tetrahedron Lett.* **2016**, *57*, 3472–3475.
- [13] M. Chakrabarty, R. Mukherjee, S. Arima, Y. Harigaya, *Heterocycles* **2009**, *78*, 139–149.
- [14] A. R. Moosavi-Zare, M. A. Zolfigol, E. Noroozizadeh, R. Salehi-Moratab, M. Zarei, *J. Mol. Catal. A: Chem.* **2016**, *420*, 246–253.
- [15] D. R. Chandam, A. A. Patravale, S. D. Jadhav, M. B. Deshmukh, *J. Mol. Liq.* **2017**, *240*, 98–105.
- [16] B. Liang, S. Kalidindi, J. A. Porco Jr, C. R. J. Stephenson, *Org. Lett.* **2010**, *12*, 572–575.
- [17] P. Anastas, N. Eghbali, *Chem. Soc. Rev.* **2010**, *39*, 301–312.
- [18] T. E. Nielsen, S. L. Schreiber, *Angew. Chem. Int. Ed.* **2008**, *120*, 52–61.
- [19] Y. Coquerel, T. Boddaert, M. Presset, D. Mailhol, J. Rodriguez, B. Pignataro, *Chemistry and Molecular Sciences Advances in Synthetic Chemistry*, VCH, Weinheim, **2010**.
- [20] S. Rostamizadeh, M. Azad, N. Shadjou, M. Hasanzadeh, *Catal. Commun.* **2012**, *25*, 83–91.
- [21] R. B. Nasir Baig, R. S. Varma, *Ind. Eng. Chem. Res.* **2014**, *53*, 18625–18629.
- [22] B. Liu, W. Zhang, F. Yang, H. Feng, X. Yang, *J. Phys. Chem. C* **2011**, *115*, 15875–15884.
- [23] R. B. Nasir Baig, R. S. Varma, *ACS Sustain. Chem. Eng.* **2014**, *2*, 2155–2158.
- [24] M. S. Ghasemzadeh, B. Akhlaghinia, *Bull. Chem. Soc. Jpn.* **2017**, *90*, 1119–1128.
- [25] T. Fey, H. Fischer, S. Bachmann, K. Albert, C. Bolm, *Org. Chem.* **2001**, *66*, 8154–8159.
- [26] V. Rackayova, C. Cudalbu, P. J. W. Pouwels, O. Braissant, *Anal. Biochem.* **2017**, *529*, 144–157.
- [27] S. S. E. Ghodsinia, B. Akhlaghinia, R. Jahanshahi, *RSC Adv.* **2016**, *6*, 63613–63623.
- [28] N. Razavi, B. Akhlaghinia, *New J. Chem.* **2016**, *40*, 447–457.
- [29] S. Rezaizadeh, B. Akhlaghinia, E. K. Goharshadi, H. Sarvari, *J. Chin. Chem. Soc.* **2014**, *61*, 1108–1114.
- [30] S. Sobhani, M. S. Ghasemzadeh, M. Honarmand, *Catal. Lett.* **2014**, *144*, 1515–1523.
- [31] M. Esmailpour, A. R. Sardarian, J. Javidi, *Appl. Catal. A: Gen.* **2012**, *445–446*, 359–367.
- [32] P. Li, Z. P. Xu, M. A. Hampton, D. T. Vu, L. Hung, V. Rodolgh, *J. Phys. Chem. C* **2012**, *116*, 10325–10332.
- [33] N. Razavi, B. Akhlaghinia, *RSC Adv.* **2015**, *5*, 12372–12381.
- [34] S. S. E. Ghodsinia, B. Akhlaghinia, *RSC Adv.* **2015**, *5*, 49849–49860.
- [35] M. Zarghani, B. Akhlaghinia, *Appl. Organomet. Chem.* **2015**, *29*, 683–689.
- [36] R. Jahanshahi, B. Akhlaghinia, *RSC Adv.* **2015**, *5*, 104087–104094.
- [37] N. Y. Siavashi, B. Akhlaghinia, M. Zarghani, *Res. Chem. Intermed.* **2016**, *42*, 5789–5806.
- [38] R. Jahanshahi, B. Akhlaghinia, *RSC Adv.* **2016**, *6*, 29210–29219.
- [39] M. Zarghani, B. Akhlaghinia, *RSC Adv.* **2016**, *6*, 31850–31860.
- [40] M. Zarghani, B. Akhlaghinia, *RSC Adv.* **2016**, *6*, 38592–38601.
- [41] S. M. Masjed, B. Akhlaghinia, M. Zarghani, N. Razavi, *Aust. J. Chem.* **2017**, *70*, 33–43.
- [42] M. Zarghani, B. Akhlaghinia, *Bull. Chem. Soc. Jpn.* **2016**, *89*, 1192–1200.
- [43] Z. Zarei, B. Akhlaghinia, *RSC Adv.* **2016**, *6*, 106473–106484.
- [44] N. Razavi, B. Akhlaghinia, R. Jahanshahi, *Catal. Lett.* **2017**, *147*, 360–373.
- [45] R. Jahanshahi, B. Akhlaghinia, *New J. Chem.* **2017**, *41*, 7203–7219.
- [46] M. Nejatianfar, B. Akhlaghinia, R. Jahanshahi, *Appl. Organomet. Chem.* **2018**, *32*, DOI 10.1002/aoc.4095.
- [47] A. Mohammadinezhad, B. Akhlaghinia, *Aust. J. Chem.* **2018**, *71*, 32–46.
- [48] A. Mohammadinezhad, B. Akhlaghinia, *Green Chem.* **2017**, *19*, 5625–5641.
- [49] Z. Zareie, B. Akhlaghinia, *New J. Chem.* **2017**, *41*, 15485–15500.
- [50] R. Jahanshahi, B. Akhlaghinia, *Catal. Lett.* **2017**, *147*, 2640–2655.
- [51] N. Mohammadian, B. Akhlaghinia, *Res. Chem. Intermed.* **2018**, *42*, 1085–1103.
- [52] Z. Zarei, B. Akhlaghinia, *Turk. J. Chem.* **2018**, *42*, 170–191.
- [53] R. A. Sheldon, *J. Mol. Catal. A* **1996**, *107*, 75–83.
- [54] Sd. Riyaz, A. Indrasena, A. Naidu, P. K. Dubey, *Indian J. Chem. B.* **2014**, *53*, 120–123.
- [55] A. Lazar, C. P. Vinod, A. P. Singh, *Micropor. Mesopor. Mat.* **2017**, *242*, 173–181.
- [56] G. Stefanovic, M. Pavicic-Woss, L. Lorenc, M. L. Mihailovic, *Tetrahedron* **1959**, *6*, 97–102.
- [57] D. Vorlander, C. Jhle, H. Volkholz, M. P. Neumann, G. von Brasche, W. Zeh, *Z Anal. Chem.* **1929**, *77*, 241.

Submitted: December 31, 2017

Revised: March 7, 2018

Accepted: March 7, 2018